

Flat band effects on the ground-state BCS-BEC crossover in atomic Fermi gases in a quasi-two-dimensional Lieb lattice

Hao Deng,^{1,2,3} Chuping Li,^{1,2,3} Yuxuan Wu,^{1,2,3} Lin Sun,^{3,2,*} and Qijin Chen^{1,2,3,†}

¹Hefei National Research Center for Physical Sciences at the Microscale and School of Physical Sciences, University of Science and Technology of China, Hefei, Anhui 230026, China

²Shanghai Research Center for Quantum Science and CAS Center for Excellence in Quantum Information and Quantum Physics, University of Science and Technology of China, Shanghai 201315, China

³Hefei National Laboratory, University of Science and Technology of China, Hefei 230088, China

(Dated: March 27, 2024)

The ground-state superfluid behavior of ultracold atomic Fermi gases with a short-range attractive interaction in a quasi-two-dimensional Lieb lattice is studied using BCS mean-field theory, within the context of BCS-BEC crossover. We find that the flat band leads to nontrivial exotic effects. As the Fermi level enters the flat band, both the pairing gap and the in-plane superfluid density exhibit an unusual power law as a function of interaction, with strongly enhanced quantum geometric effects, in addition to a dramatic increase of compressibility as the interaction approaches the BCS limit. As the Fermi level crosses the van Hove singularities, the character of pairing changes from particle-like to hole-like or vice versa. We present the computed phase diagram, in which a pair density wave state emerges at high densities with relatively strong interaction strength.

I. INTRODUCTION

Ultracold atomic Fermi gases in optical lattices have become an ideal platform for quantum simulation and quantum engineering and thus have enormous potential for exploring difficult condensed matter problems and new quantum physics [1–5], due to their multiple adjustable parameters, including interaction strength, lattice depth, dimensionality, population imbalance, and lattice geometry, etc [6–10]. In particular, crossover from a BCS type of superfluidity to Bose–Einstein condensation (BEC) of fermion pairs in an attractive Hubbard model can be realized in an optical lattice using atomic Fermi gases in an optical lattice [11]. Such a BCS-BEC crossover has been realized by tuning the effective interaction strength through a Feshbach resonance in trapped atomic Fermi gases [12]. Such studies can help to elucidate the underlying physics of the widespread pseudogap phenomena in cuprate superconductors [13], which is of central importance in understanding the mechanism of high-temperature superconductivity [14].

Recently, models with a flat band have attracted great interest, because of the associated high density of states (DOS) and possible quantum geometric effect associated with multiband of such systems. It has been reported that flat band and quantum geometric effect may enhance the superconducting transition temperature with an on-site attractive interaction and may give rise to quantum Hall states with a nonzero Chern number [15–20]. Flat bands have been studied in bipartite lattices, e.g., Lieb lattice, magic-angle graphene moiré lattices, as well as perovskite, kagome and honeycomb lattices [15, 21–24].

Particularly, Lieb lattices have been realized in optical lattices of ultracold atoms [25, 26]. With line centers on a square, a Lieb lattice contains a central flat band, which touches an upper and a lower band at the Dirac points at the Brillouin zone corners [27]. There have been a number of theoretic

cal and experimental studies on Lieb lattices, including lattice preparation [25, 26, 28] and associated aspects such as Chern semimetals with three spinless fermion species [29], ferromagnetic and antiferromagnetic states in a repulsive Hubbard model at half filling [30–32], strain-induced superconductor-insulator transition [33], competition between pairing and charge density wave at half filling using determinant quantum Monte Carlo [34], as well as topologically nontrivial quantum spin Hall effect with extra interactions [19, 35–37]. Such rich physics warrants the investigation of the important superfluidity and pairing phenomenon of ultracold Fermi gases in a Lieb lattice, in order to uncover possible exotic and interesting new quantum phenomena in the presence of a flat band.

In this Letter, we investigate the flat band effects on the ground-state superfluid behaviors of ultracold atomic Fermi gases in a quasi-two-dimensional Lieb lattice with a short-range attractive interaction, with the nearest neighbor hopping only, which leads to a zero Chern number [38]. We find that the flat band, as well as the van Hove singularities (VHS), leads to exotic phenomena in the superfluid behavior. When the Fermi level enters the flat band, the fermion pairing gap Δ changes from an exponential dependence into an unusual power law, as a function of the interaction strength $|g|$, with an enormous compressibility κ in the BCS limit. The superfluid density also exhibits a power law behavior, in contrast to being a constant in 3D free space. For a lower number density n slightly above 1 fermion per unit cell, the fermion chemical potential μ varies *nonmonotonically* with the interaction strength in the weak interaction region, and reaches a maximum when it crosses the VHS, signaling a change of pairing character from particle-like at strong interactions to hole-like at weak interactions. At the same time, κ rises in the weak coupling region as the Fermi level gets closer to the VHS. In the BEC regime, μ shows an asymptotic linear dependence on the interaction g , leading to a density-independent $\kappa = -2/g$, with the pairing gap $\Delta \sim |\mu| \sim |g|$, which is qualitatively similar to the 3D lattice case [39]. Finally, the phase diagram reveals that a pair density wave (PDW) ground state emerges at intermediate pairing strength for relatively large densities,

* Corresponding author: lsun22@ustc.edu.cn

† Corresponding author: qjc@ustc.edu.cn

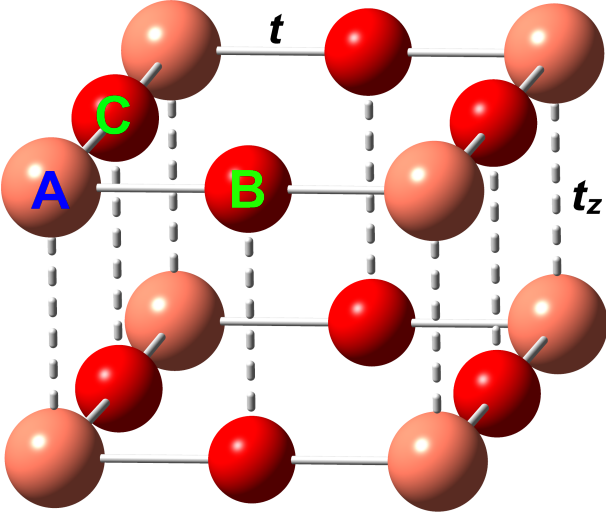


Figure 1. Structure of a quasi-2D Lieb lattice. Site A represents the site in a simple square lattice, while sites B and C sit at the line centers of the square in each 2D plane. The solid lines represent nearest-neighbor hopping integral t between site A and sites B and C. The dashed lines denote the inter-layer coupling t_z .

due to strong inter-pair repulsive interactions and relatively large pair size at intermediate pairing strength, which is also found in dipolar Fermi gases [40] and Fermi gases in 2D optical lattices with one continuum dimension [41, 42] within the pairing fluctuation theory.

II. THEORETICAL FORMALISM

The non-interacting Hamiltonian of a Lieb lattice can be written as

$$H_0 = \sum_{\mathbf{k}\sigma} \hat{c}_{\mathbf{k}\sigma}^\dagger \hat{H}_{\mathbf{k}} \hat{c}_{\mathbf{k}\sigma},$$

where $\hat{c}_{\mathbf{k}\sigma} = [C_{A\mathbf{k}\sigma}, C_{B\mathbf{k}\sigma}, C_{C\mathbf{k}\sigma}]^T$. The subscript A denotes the site in a standard square lattice with B and C located on the side center of the square, as shown in Fig. 1. This leads to the Hamiltonian in momentum space for free fermions

$$\hat{H}_{\mathbf{k}} = \begin{bmatrix} d_k & a_k & b_k \\ a_k & d_k & 0 \\ b_k & 0 & d_k \end{bmatrix},$$

where $a_k = 2t[1 - \cos(k_x/2)]$, $b_k = 2t[1 - \cos(k_y/2)]$ and $d_k = 2t_z(1 - \cos k_z) - \mu$ represent the hopping in the x and y directions, and the dispersion in the out-of-plane \hat{z} direction, respectively, with t and t_z being the in-plane and out-of-plane hopping integral, respectively. We take $t_z/t = 0.01$ for the quasi-two dimensionality, set the lattice constant $a = 1$, and measure energy relative to the bottom of the lower energy band. Diagonalizing $\hat{H}_{\mathbf{k}}$ leads to three bands with dispersions $\xi_{\mathbf{k}}^\alpha = \alpha\sqrt{2}t\sqrt{2 + \cos k_x + \cos k_y} + 2\sqrt{2}t + 2t_z(1 - \cos k_z) - \mu$, where $\alpha = \pm, 0$ denotes the upper, lower and flat band, respectively. This yields in the band representation

$H_0 = \sum_{\mathbf{k}\alpha\sigma} \xi_{\mathbf{k}}^\alpha c_{\mathbf{k}\alpha\sigma}^\dagger c_{\mathbf{k}\alpha\sigma}$, where $c_{\mathbf{k}\alpha\sigma}$ is the annihilation operator in band α .

The interaction Hamiltonian in the band representation is given by

$$H_{\text{int}} = \sum_{\mathbf{k}\mathbf{k}'\mathbf{q}\alpha\beta} U_{\mathbf{k}\mathbf{k}'\alpha\beta} c_{\mathbf{k}+\frac{\mathbf{q}}{2}\alpha\uparrow}^\dagger c_{-\mathbf{k}+\frac{\mathbf{q}}{2}\alpha\downarrow}^\dagger c_{-\mathbf{k}'+\frac{\mathbf{q}}{2}\beta\downarrow} c_{\mathbf{k}'+\frac{\mathbf{q}}{2}\beta\uparrow},$$

with band indices $\alpha, \beta = \pm, 0$. The full Hamiltonian is thus $H = H_0 + H_{\text{int}}$. We find that with only on-site interactions, the pairing gap often varies strongly from site to site [43], which necessarily leads to a large kinetic energy for the pairing field, and thus may not be energetically favorable in the superfluid state. Since the nearest-neighbor hopping hybridizes different orbitals, and to be compatible with the conventional superconductivity with electron-phonon interaction induced pairing, we find it reasonable to assume a uniform short-range intra- and inter-orbital interaction, $U_{ij} = U$, where $i, j = \{A, B, C\}$ are the orbital indices. Through a unitary transformation, this leads naturally to uniform matrix elements of the interaction in momentum space across all bands, with $U_{\mathbf{k}\mathbf{k}'\alpha\beta} = g < 0$. (See Appendix A for details). This in turn gives rise to a uniform order parameter $\Delta_\alpha = \Delta$ in the mean field approximation [44]. We emphasize that, despite the short interaction range, fermion hopping enables pairing between sites across a large distance.

Using the BCS mean-field theory at zero temperature, the bare and full Green's functions are given by

$$G_0(K) = \frac{\theta(|k| - k_F)}{\omega - \hat{H}_{\mathbf{k}} + i0^+} + \frac{\theta(k_F - |k|)}{\omega - \hat{H}_{\mathbf{k}} - i0^+},$$

$$G^{-1}(K) = G_0^{-1}(K) - \Sigma(K), \quad \Sigma(K) = -\Delta^2 G_0^T(-K),$$

respectively, with four momentum $K \equiv (\omega, \mathbf{k})$, and $\theta(x)$ is the step function.

The number constraint $n = 2 \sum_K \text{Tr} G(K)$ leads to the number equation

$$n = \sum_{\mathbf{k}} \sum_{\alpha=0,\pm} \left(1 - \frac{\xi_{\mathbf{k}}^\alpha}{E_{\mathbf{k}}^\alpha} \right), \quad (1)$$

where $\sum_K \equiv \sum_\omega \sum_{\mathbf{k}}$, and $E_{\mathbf{k}}^\alpha = \sqrt{(\xi_{\mathbf{k}}^\alpha)^2 + \Delta^2}$ is the Bogoliubov quasiparticle dispersion for band $\alpha = \pm, 0$ with energy gap Δ . The gap equation is given by [44]

$$0 = \frac{1}{g} + \sum_{\mathbf{k}} \sum_{\alpha=0,\pm} \frac{1}{2E_{\mathbf{k}}^\alpha}. \quad (2)$$

Equations (1) and (2) form a closed set of self-consistent equations, which can be solved for (μ, Δ) as a function of g in the superfluid phase. The solution for (μ, Δ) in the superfluid phase should satisfy the stability condition that the Cooper pair energy should be nonnegative. To this end, we extract the pair dispersion using the fluctuating pair propagator, as given in the pairing fluctuation theory which was previously developed for the pseudogap physics in the cuprates [14], and extended to address the BCS-BEC crossover in atomic

Fermi gases [1]. To be compatible [45] with the BCS-Leggett ground state, the pair susceptibility in the T -matrix $t_{\text{pg}}^{-1}(Q) = 1/g + \chi(Q)$ is given by $\chi(Q) = \sum_{\mathbf{K}} \text{Tr} [G(\mathbf{K})G_0^T(Q - \mathbf{K})]$, with $Q \equiv (\Omega, \mathbf{q})$, which leads to $t_{\text{pg}}^{-1}(\Omega, \mathbf{q}) \approx a_0(\Omega - \Omega_{\mathbf{q}})$, with pair dispersion $\Omega_{\mathbf{q}} = 2B(2 - \cos q_x - \cos q_y) + 2B_z(1 - \cos q_z)$. Here B and B_z correspond to the effective pair hopping integral in the xy plane and in the z direction, respectively. The expressions for the coefficients a_0 , B and B_z can be readily derived during the Taylor expansion. The non-negativeness of the pair dispersion requires that the pairing correlation length (squared) $\xi^2 = a_0B$ and $\xi_z^2 = a_0B_z$ be positive.

Superfluid density (n_s/m) is an important transport property; its dependence on the interaction often reflects the pairing symmetry. It takes the average of the inverse band mass in a lattice, in contrast with the 3D continuum case where it is always given by n/m at $T = 0$ in BCS theory. Moreover, the in-plane component of (n_s/m) can be divided into a conventional and a geometric part, due to the presence of the flat band, where the geometric term is associated with the interband contributions, which are proportional to a quantum metric tensor.

The expressions for the superfluid density (n_s/m) are derived using the linear response theory within the BCS framework [46, 47], which is applied to the multi-band system [48][49]. Similar to Ref. [48], the in-plane superfluid density (n_s/m) $_{\parallel}$ contains a conventional term (n_s/m) $_{\parallel}^{\text{conv}}$ and a geometric term (n_s/m) $_{\parallel}^{\text{geom}}$, i.e.,

$$\left(\frac{n_s}{m}\right)_{\parallel} = \left(\frac{n_s}{m}\right)_{\parallel}^{\text{conv}} + \left(\frac{n_s}{m}\right)_{\parallel}^{\text{geom}}, \quad (3)$$

where

$$\left(\frac{n_s}{m}\right)_{\parallel}^{\text{conv}} = \frac{t^2}{4} \sum_{\mathbf{k}} \sum_{\alpha=\pm} \frac{\Delta^2}{(E_{\mathbf{k}}^{\alpha})^3} \frac{\sin^2 k_x + \sin^2 k_y}{2 + \cos k_x + \cos k_y}, \quad (4)$$

$$\left(\frac{n_s}{m}\right)_{\parallel}^{\text{geom}} = \Delta^2 \sum_{\mathbf{k}} \left[\left(\frac{1}{E_{\mathbf{k}}^+} - \frac{1}{E_{\mathbf{k}}} \right) \frac{\xi_{\mathbf{k}} - \xi_{\mathbf{k}}^+}{\xi_{\mathbf{k}} + \xi_{\mathbf{k}}^+} + \left(\frac{1}{E_{\mathbf{k}}^-} - \frac{1}{E_{\mathbf{k}}} \right) \frac{\xi_{\mathbf{k}} - \xi_{\mathbf{k}}^-}{\xi_{\mathbf{k}} + \xi_{\mathbf{k}}^-} \right] (g_{xx} + g_{yy}). \quad (5)$$

Here $g_{\mu\nu} = \text{Re}(\partial_{\mu}\langle + |)(1 - |+\rangle\langle + |)\partial_{\nu}|+\rangle)$ is the quantum metric tensor of the upper or lower band, where $|\pm\rangle$ is the eigenvector of $\hat{H}_{\mathbf{k}}$, associated with the upper and lower bands, respectively. The out-of-plane component reads

$$\left(\frac{n_s}{m}\right)_z = 2t_z^2 \sum_{\mathbf{k}} \sum_{\alpha=0,\pm} \frac{\Delta^2}{(E_{\mathbf{k}}^{\alpha})^3} \sin^2 k_z. \quad (6)$$

Note that, without using the mean-field approximated Hamiltonian, we do not find the extra contributions to n_s/m associated with the derivative of Δ with respect to the magnetic field vector potential, unlike Ref. [50].

Compressibility κ is an important quantity in thermodynamics, which must be positive to maintain mechanical sta-

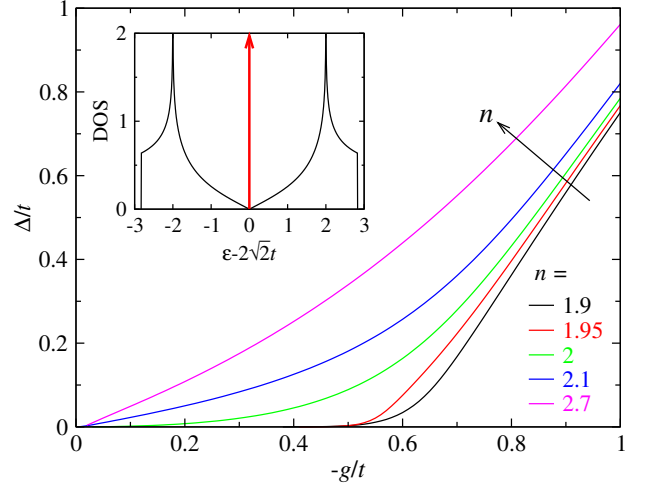


Figure 2. Δ as a function of $-g$ for various n in the weak coupling BCS regime, with μ close to or inside the flat band. Shown in the inset is the DOS for strict 2D, where the (red) arrow denotes the flat band.

bility. For the ground state [51], we obtain

$$\begin{aligned} \kappa &= \frac{\partial n}{\partial \mu} = \left(\frac{\partial n}{\partial \mu} \right)_{\Delta} + \left(\frac{\partial n}{\partial \Delta} \right)_{\mu} \frac{\partial \Delta}{\partial \mu} \\ &= \sum_{\mathbf{k}\alpha} \frac{\Delta^2}{(E_{\mathbf{k}}^{\alpha})^3} + \frac{[\sum_{\mathbf{k}\alpha} \xi_{\mathbf{k}}^{\alpha}/(E_{\mathbf{k}}^{\alpha})^3]^2}{\sum_{\mathbf{k}\alpha} 1/(E_{\mathbf{k}}^{\alpha})^3}. \end{aligned} \quad (7)$$

One can tell that κ reflects the property of density of state (DOS). In the weak coupling regime, a larger DOS at the Fermi level corresponds to a higher κ . Especially, κ reduces to the DOS in the noninteracting limit.

The asymptotic behavior in the BEC limit can be solved analytically with large negative $\mu \rightarrow -\infty$. The gap and number equations yield

$$\mu = \frac{(3-n)g}{2} + 2\sqrt{2}t, \quad \Delta = \sqrt{\frac{9}{4}g^2 - \mu^2}, \quad (8)$$

respectively, with a scaling behavior qualitatively similar to $\Delta \sim |\mu| \sim |g|$ for 3D lattice. Thus, we obtain for all densities the BEC asymptote

$$\kappa = -\frac{2}{g}. \quad (9)$$

III. NUMERICAL RESULTS AND DISCUSSIONS

We first investigate the flat band effects on the pairing gap behavior, when the Fermi level is close to or within the flat band. Due to the particle-hole symmetry, we *restrict* ourselves to $n \leq 3$, and the Fermi level enters the flat band for $n \geq 2$ in the noninteracting limit. Plotted in Fig. 2 is Δ versus $-g$ (in units of t) for various densities near $n \lesssim 2$ and $n \in [2, 3]$ in the weak coupling BCS regime. Shown in the inset is the DOS for the strict 2D case, where the (red) vertical arrow denotes the flat band, along with two VHS's in the upper and

lower bands, corresponding to $n = 1$ and 5 , respectively. For $n < 2$, including $n = 1.95$, Δ exhibits an exponentially activated behavior in the weak coupling regime, similar to that in 3D continuum and 3D cubic lattices. This is expected in BCS theory, assuming a roughly constant DOS near the Fermi surface. However, as the density n goes above 2, the Fermi level enters the flat band with the lower band fully filled, and the gap $\Delta(g)$ as a function of the interaction exhibits an unusual power law, which can be attributed to the breakdown of the constant DOS approximation. Similar behavior has also been predicted within the dynamical mean-field theory in a quasi 2D *repulsive* Lieb lattice, where the magnetism as a function of the interaction g changes from exponential to power law behavior at half filling [31]. The behavior of Δ over a broad range is shown in the inset of Fig. 3(b) on a log-log scale for a lower density, $n = 0.6$. Indeed, the numerical result (black solid line) approaches its analytical BEC asymptote (red dashed line) in the deep BEC regime, as given by Eq. (8).

This unusual power-law behavior of Δ versus g can be explained following Ref. [31], despite the different signs of the interaction. Using the normalized, dimensionless notation $\bar{X} \equiv X/W$, where $W = 4\sqrt{2}t + 4t_z$ is the bandwidth, the rescaled, dimensionless DOS can be simplified as $\bar{\rho}(\bar{\varepsilon}) \equiv W\rho(\bar{\varepsilon}) = 4\theta(1/2 - |\bar{\varepsilon} - 1/2|) + 2\delta(\bar{\varepsilon} - 1/2)$, where the δ function represents the flat band.

For $n > 2$, using $\bar{\rho}(\bar{\varepsilon})$ in the integral in the gap equation (2), we obtain from the gap equation (2)

$$\bar{\Delta} = \frac{n-2}{8} / \mathcal{W}\left(\frac{n-2}{8} \exp\left(\frac{1}{4|\bar{g}|}\right)\right),$$

where \mathcal{W} is the Lambert \mathcal{W} -function, which is the inverse function of $f(\mathcal{W}) = \mathcal{W} \exp(\mathcal{W})$ (See Appendix B for a derivation). For $x \gg 1$, $\mathcal{W}(x) \approx \ln(x) - \ln(\ln(x))$. To leading order, this yields $\bar{\Delta} \approx \frac{n-2}{2} |\bar{g}|$ for weak interactions. At low $n < 2$, the δ -function term in $\bar{\rho}(\bar{\varepsilon})$ becomes irrelevant, so that we recover the ordinary exponential BCS behavior.

Next we show in Fig. 3 the behaviors of μ as a function of g for various densities n , so that the Fermi level changes from (a) the lower band below ($n = 0.6$) and around the VHS ($0.9 \leq n \leq 1.2$) to (b) near ($n = 1.9, 1.95$) or inside the flat band ($n = 2, 2.3, 2.7$). As shown in the inset of Fig. 3(a), $-\mu$ (black solid line, for $n = 0.6$) approaches its BEC asymptotic behavior (red dashed line) for $-g/t > 10$. For $n \leq 1$ in Fig. 3(a), the chemical potential μ decreases monotonically as the pairing interaction becomes stronger, similar to that in a regular one-band model below half filling. However, for $n = 1.1, 1.2$, μ becomes remarkably nonmonotonic in the weak coupling regime; μ increases first with $|g|$, and then starts to decrease after passing a maximum. Such nonmonotonicity is also found in a 2D optical lattice with a strong lattice effect, which is comprised of two lattice and one continuum dimensions [41, 42]. In a quasi-2D Lieb lattice, the lower band has two VHS's, at $\varepsilon = (2\sqrt{2} - 2)t \approx 0.8284t$ and $\varepsilon = (2\sqrt{2} - 2)t + 4t_z \approx 0.8684t$. For $n = 1.1, 1.2$, $\mu > 0.8684t$ for small $|g|$, i.e., the Fermi level sits slightly above the VHS's for small $|g|$, where the DOS $\rho(\varepsilon)$ has a negative slope, so that the pairing becomes hole-like, for which

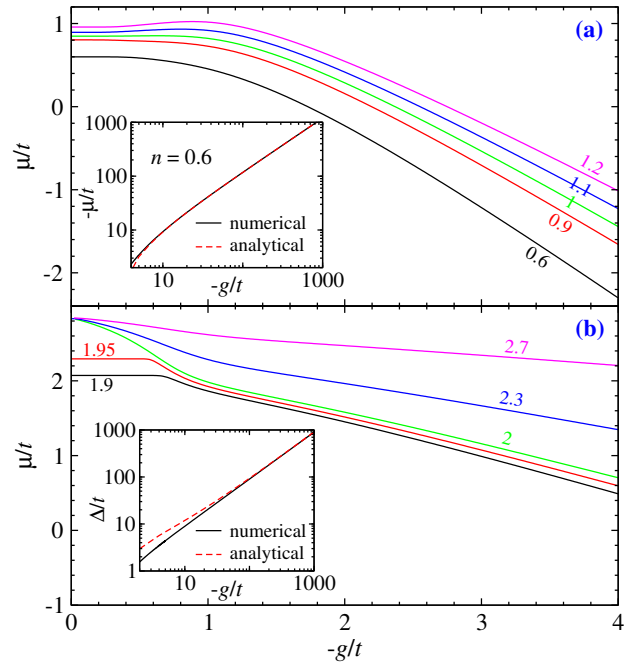


Figure 3. Evolution of μ as a function of $-g/t$ for (a) small $0.6 \leq n \leq 1.2$ and (b) large $1.9 \leq n \leq 2.7$, as labeled. In the insets, the full numerical solution (black solid) for $n = 0.6$ is compared with the analytical BEC asymptotic behavior (red dashed curves) for $-\mu$ and Δ , respectively, as a function of $-g/t$ on a log-log scale.

μ increases as the pairing becomes stronger, as in a 3D cubic lattice *above* half filling. Indeed, in the *weak* coupling limit, there is generally an approximate particle-hole symmetry at the VHS, as the DOS in the vicinity of the VHS's dominates. As $|g|$ increases further, the contribution of the DOS below the VHS's comes in, so that μ starts to decrease again. As n increases and approaches $n = 2$, the flat band gradually affects the behaviors of μ in the BCS regime. For $n = 1.9, 1.95$ in Fig. 3(b), μ remains nearly a constant before decreasing with $|g|$ in the BCS regime. For $2 \leq n \leq 3$, μ enters the flat band, and starts to decrease from roughly the same non-interacting limit $\mu_0 \approx 2\sqrt{2}t$. While the nearly constant μ for $n = 1.9, 1.95$ is in accord with the exponentially small gap in the BCS regime (Fig. 2), a power-law decrease in μ can be readily seen for $n \in [2, 3]$, commensurate with the power-law increase of Δ as a function of $-g$.

Shown in Fig. 4 are the in-plane (left column) and out-of-plane (right column) superfluid density, from top to bottom, for $n = 0.6, 2$ and 2.7 , respectively, as well as the conventional $(n_s/m)_{\parallel}^{\text{conv}}$ (blue) and geometric part $(n_s/m)_{\parallel}^{\text{geom}}$ (red curves) of $(n_s/m)_{\parallel}$. For $n = 0.6$, both the in-plane $(n_s/m)_{\parallel}$ and the out-of-plane $(n_s/m)_z$, as well as the conventional $(n_s/m)_{\parallel}^{\text{conv}}$, are roughly constant for weak coupling, similar to the constant superfluid density $n_s/m = n/m$ in 3D continuum. On the contrary, the geometric part $(n_s/m)_{\parallel}^{\text{geom}}$ vanishes in the noninteracting limit $g \rightarrow 0$. Commensurate with the evolution of Δ versus $-g$, as n increases to $n \geq 2$, the behaviors of both $(n_s/m)_{\parallel}^{\text{conv}}$ and $(n_s/m)_{\parallel}^{\text{geom}}$, as well as

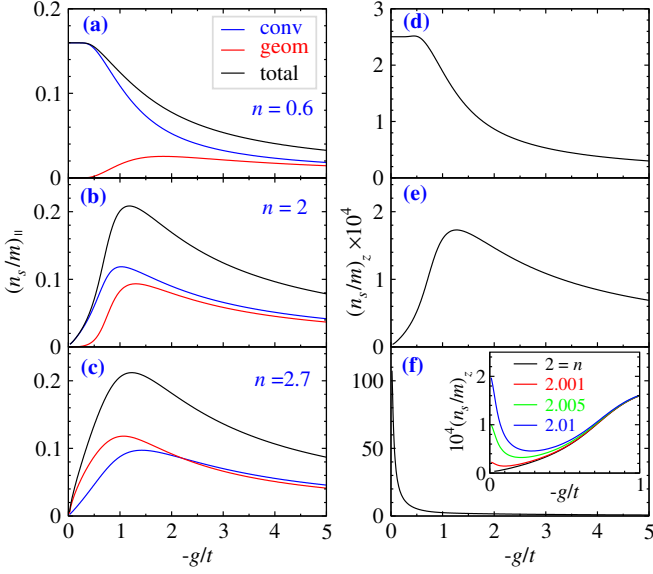


Figure 4. Behavior of the in-plane superfluid density $(n_s/m)_\parallel$ (black curves) along with its conventional (blue curves) and geometric parts (red curves), as a function of $-g/t$, for (a) $n = 0.6$, (b) 2, (c) 2.7. Plotted in (d-f) are the corresponding out-of-plane superfluid density $(n_s/m)_z$. Shown in the inset of panel (f) is $(n_s/m)_z$ in the weak interaction regime for a series of $n \gtrsim 2$.

$(n_s/m)_\parallel$, evolve into power laws as a function of $-g$. More importantly, $(n_s/m)_\parallel^{\text{conv}}$ now approaches zero as $g \rightarrow 0$, unlike in a simple cubic lattice. This can be attributed to a few reasons. (i) Without the out-of-plane contribution, the DOS from the upper and lower band is zero when μ falls inside the flat band. (ii) There is a perfect particle-hole symmetry at this μ so that the contributions from particles and holes cancel out in $(n_s/m)_\parallel$; the pairing is neither particle-like nor hole-like. (iii) The quantum geometric contribution relies on a finite gap Δ , and hence vanishes in the zero g limit. (iv) The flat band does not contribute to superfluidity without the quantum geometric effect. As μ moves away from the flat band with increasing $|g|$, the particle-hole cancellation breaks down, leading to a rising $(n_s/m)_\parallel$. As $|g|$ increases further toward the BEC regime, $(n_s/m)_\parallel$ starts to decrease due to the lattice effects. Without a geometric contribution, the out-of-plane superfluid density $(n_s/m)_z$ exhibits a behavior similar to that of $(n_s/m)_\parallel^{\text{conv}}$ in the weak coupling regime for $n = 0.6$ and 2. However, difference appears as μ enters the flat band. As shown in the inset of Fig. 4(f), when n becomes slightly higher than 2, $(n_s/m)_z$ starts to increase as $g \rightarrow 0$. At $n = 2.7$, shown in Fig. 4(f), this increase is so dramatic that $(n_s/m)_z$ becomes monotonically decreasing with $|g|$. This distinct behavior of $(n_s/m)_z$, compared to $(n_s/m)_\parallel^{\text{conv}}$, results from the broadening of the flat band due to the small out-of-plane dispersion.

Plotted in Fig. 5 is the compressibility κ versus g for (a) small n below and around the VHS and (b) large n near and in the flat band. Figure 5(a) indicates that the noninteracting value of κ reaches a local maximum at the VHS $n = 1$ as a function of n , since this value is given by the DOS. Further-

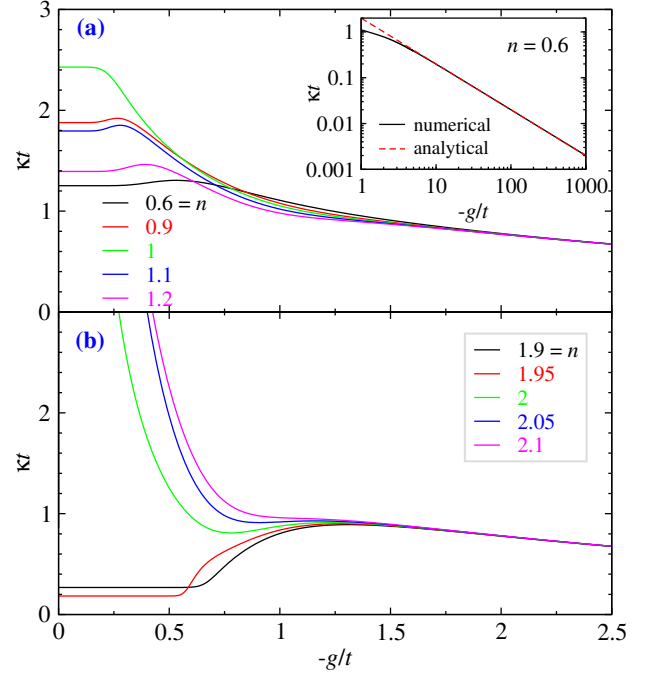


Figure 5. κ versus $-g$ for (a) small n below ($n = 0.6$) and close to the VHS's around $n = 1$ and (b) large $n \simeq 2$ near the flat band bottom. Shown in the inset is the full numerical solution of $\kappa(g)$ (black solid), compared with its BEC asymptotic expression $\kappa = -2/g$ (red dashed curve) for $n = 0.6$ on a log-log scale.

more, for $n \in [0.9, 1.2]$, κ varies nonmonotonically with g , largely related to the nonmonotonic behavior of $\mu(g)$. As $|g|$ increases into the BEC regime, all fermions pair up and the two-body binding energy dominates μ . Consequently, κ decreases and approaches the same n -independent BEC asymptote. Indeed, as shown in the inset for $n = 0.6$, κ approaches nicely the n -independent analytical BEC asymptote when $-g/t > 10$. The nearly constant κ for $n = 1.9$ and 1.95 in Fig. 5(b) is clearly associated with the constant behavior of μ in the BCS regime shown in Fig. 3(b). For $n \geq 2$, κ increases sharply as $g \rightarrow 0$. Here the Fermi level falls within the flat band, and thus the noninteracting κ is given by the huge DOS. Therefore, there is a jump of $\kappa(g = 0)$ as n crosses the $n = 2$ boundary, as shown in Fig. 5(b).

Finally, we present in Fig. 6 the ground-state phase diagram in the $n - g$ plane. Here the positivity of $\xi^2 = a_0 B$ and $\xi_z^2 = a_0 B_z^2$ constitutes two stability conditions for the superfluid phase. The (black dot-dashed) $\mu = 0$ curve separates the fermionic superfluid regime on the upper left from the bosonic superfluid regime on the lower right. A PDW ground state with negative $\xi^2 < 0$ and/or $\xi_z^2 < 0$ emerges in the grey shaded region, enclosed inside the (red) $B = 0$ and (blue) $B_z = 0$ curves. Note that the upper branch of $B = 0$ overlaps nearly precisely with $B_z = 0$, and both are close to but falls slightly inside the fermionic side of the $\mu = 0$ line. The PDW state at intermediate and strong coupling for relatively large n is associated with the strong repulsive inter-pair interaction U and relatively low kinetic energy of the pairs, T , which leads

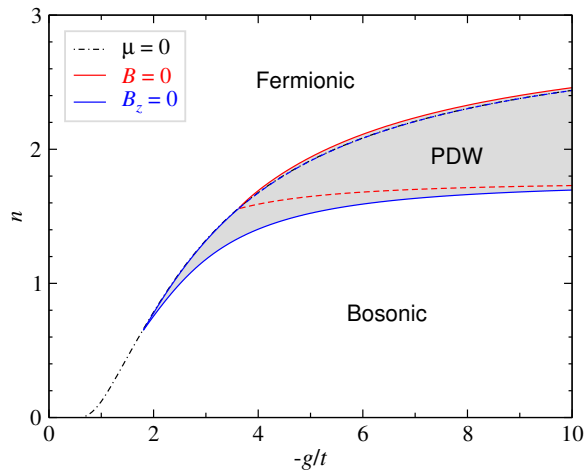


Figure 6. Ground-state phase diagram in the $n - g$ plane. The (black dot-dashed) $\mu = 0$ curve divides the plane into fermionic and bosonic superfluid regimes. Enclosed within the (red) $B = 0$ and (blue) $B_z = 0$ lines is a PDW ground state (gray shaded region).

naturally to Wigner crystallization. Indeed, for N pairs, the inter-pair interaction energy E_P scales as $N^2U/2$ whereas the kinetic energy E_K scales as NT , allowing $E_P > E_K$ with a large U and lattice suppressed T . Technically, the sign of ξ^2 (or ξ_z^2) becomes negative between the $B = 0$ (or $B_z = 0$) branches, where the pair dispersion $\tilde{\Omega}_{\mathbf{q}}$ reaches a minimum at a finite $\mathbf{q} \neq 0$, with the crystallization wave vector in the xy plane (or in the z direction). The PDW state has been observed in experiments [52], but it is still unclear whether it can sustain superfluidity and thus becomes a supersolid, which will be left to a future study. A similar PDW ground state has been found in 3D lattices at high density [39], 2D optical lattices with strong lattice effect [41, 42], optical lattices in mixed dimensions [53], and in dipolar Fermi gases [40].

IV. CONCLUSIONS

In summary, we have studied the ground-state superfluid properties of ultracold Fermi gases in a quasi-2D Lieb lattice in the context of BCS-BEC crossover, whose BEC asymptotic solution is derived analytically. We find that the flat band, together with van Hove singularities, have extraordinary effects on the superfluid behavior. When the Fermi level falls within the flat band, the pairing gap and the in-plane superfluid density exhibit an unusual power law in the weak coupling regime as a function of the interaction strength $|g|$. Meanwhile, the compressibility increases sharply in the noninteracting limit. As the chemical potential increases across the VHS's in the lower band, the pairing becomes hole-like for weak interactions, leading to a nonmonotonic behavior of the chemical potential as a function of interaction strength. A PDW ground state emerges for intermediate and strong pairing strength with relatively large density. These findings for the Lieb lattice are very different from that for pure 3D continua and 3D cubic lattices and should be tested in future ex-

periments.

V. ACKNOWLEDGMENTS

This work was supported by the Innovation Program for Quantum Science and Technology (Grant No. 2021ZD0301904).

Appendix A: Motivation of uniform interaction across the energy bands

The attractive Hubbard model, often written in a single-band form, has been used as a formulation for superconductors in both the weak and strong coupling regimes. For a typical conventional superconductor with a pairing interaction of the electron-phonon origin, the pairing “glue” was mediated via the retarded ionic lattice deformation, causing electrons in the vicinity of the Fermi surface to form Cooper pairs of nearly zero center-of-mass momentum. This effective pairing interaction, originated from the Coulomb potential induced by nonzero net charge at the deformed ion sites, necessarily propagates over a large distance, allowing for large Cooper pairs in real space. Clearly, such a Coulomb force does not distinguish between different sublattice sites in the multi-orbital situation, such as the Lieb lattice. While the simplest one-band Hubbard model usually considers only on-site interactions, the fact that the order parameter is spatially uniform in a conventional superconductor allows one to obtain the correct result by assuming local on-site pairing, even if the electron-phonon interaction is in fact effective across a distance.

However, such a picture may breakdown for a multi-orbital model, if one considers on-site attraction only. Indeed, this would lead to orbital selective pairing interaction, which may not necessarily be equal to each other. Therefore, the order parameter necessarily varies from site to site. An example can be seen from Ref. [43]. This implies a high kinetic energy for the pairing field Ψ , associated with the $|\nabla\Psi|^2$ term in the Ginzburg-Landau free energy. This is clearly not energetically favorable for forming a uniform superfluid. It suggests that for a conventional superconductor, one needs to consider inter-orbital pairing interaction as well. Given the large Cooper pair size, there is essentially no real-space *local* on-site pairing. Thus to make the multi-orbital Hubbard model work for weak attractions, it is desirable to assume a uniform inter-orbital and on-site interaction. (Here the “on-site” should be replaced by “intra-orbital”). Therefore, we argue that it is appropriate to use a uniform pairing interaction that does not distinguish between intra- and inter-orbitals. This in return leads to a uniform pairing interaction across all energy bands. This can be readily seen as the band representation and the orbital representation are related via a simple unitary basis transformation.

We also note that with the nearest neighbor approximation, fermion hopping occurs between different sublattice sites. Therefore, the orbital index is not a good quantum number. It is in the band index that the (bare) Hamiltonian is diagonalized. It is thus not ideal to define the order parameter in terms

of the orbitals. The BCS pairing couples fermions of (nearly) opposite momenta near the Fermi level, irrespective their orbital origin. This necessarily mixes different orbitals, as the three band dispersions clearly differ dramatically from those of each orbital alone.

The fermion creation/annihilation operators are in the band and orbital representations are related via a unitary transformation, $C_{\mathbf{k}i\sigma} = \sum_{\alpha} S_{i\alpha}(\mathbf{k})C_{\mathbf{k}\alpha\sigma}$, where $i = A, B, C$ refers to the orbitals, and $\alpha = \pm, 0$ is the band index. For the simple Lieb lattice, the transform matrix $S(\mathbf{k}) = S(-\mathbf{k}) = S^{\dagger}(\mathbf{k})$ is real, satisfying $S^{\dagger}(\mathbf{k})S(\mathbf{k}) = 1$.

With a short-range interaction that does not distinguish between inter- and intra-orbitals, namely $U_{ij} = U_{ii} = U$, we readily write down the two-body interaction matrix element in the momentum space in the center-of-mass reference frame, in terms of the orbitals,

$$\begin{aligned} H_{\mathbf{k}\mathbf{k}'}^{\text{int}} &= U \sum_{ij} C_{\mathbf{k}i\uparrow}^{\dagger} C_{-\mathbf{k}i\downarrow}^{\dagger} C_{-\mathbf{k}'j\downarrow} C_{\mathbf{k}'j\uparrow} \\ &= U \left[\sum_{\alpha_3\alpha_4} S_{i\alpha_4}(\mathbf{k}) S_{i\alpha_3}(\mathbf{k}) C_{\mathbf{k}\alpha_4\uparrow}^{\dagger} C_{-\mathbf{k}\alpha_3\downarrow}^{\dagger} \right] \\ &\quad \times \left[\sum_{\alpha_1\alpha_2} S_{j\alpha_1}(\mathbf{k}') S_{j\alpha_2}(\mathbf{k}') C_{-\mathbf{k}'\alpha_1\uparrow} C_{\mathbf{k}'\alpha_2\downarrow} \right] \\ &= U \left(\sum_{\alpha_3\alpha_4} \delta_{\alpha_3\alpha_4} C_{\mathbf{k}\alpha_4\uparrow}^{\dagger} C_{-\mathbf{k}\alpha_3\downarrow}^{\dagger} \right) \left(\sum_{\alpha_1\alpha_2} \delta_{\alpha_1\alpha_2} C_{-\mathbf{k}'\alpha_1\uparrow} C_{\mathbf{k}'\alpha_2\downarrow} \right) \\ &= U \sum_{\alpha\beta} C_{\mathbf{k}\beta\uparrow}^{\dagger} C_{-\mathbf{k}\beta\downarrow}^{\dagger} C_{-\mathbf{k}'\alpha\downarrow} C_{\mathbf{k}'\alpha\uparrow}, \end{aligned}$$

which has been transformed into the band representation in the last line with a uniform interaction across all bands. Here \mathbf{k}' and \mathbf{k} are the relative momentum (divided by 2) for the incoming and outgoing scattering fermions, respectively.

Now with the uniform pairing interaction across bands, $U_{\mathbf{k}\mathbf{k}'\alpha\beta} = g < 0$, and defining in the band representation the order parameter

$$\begin{aligned} \Delta_{\mathbf{k}}^{\alpha} &= - \sum_{\beta\mathbf{k}'} U_{\mathbf{k}\mathbf{k}'\alpha\beta} \langle c_{-\mathbf{k}\beta\downarrow} c_{\mathbf{k}\beta\uparrow} \rangle \\ &= -g \sum_{\beta\mathbf{k}'} \langle c_{-\mathbf{k}'\beta\downarrow} c_{\mathbf{k}'\beta\uparrow} \rangle = \Delta, \end{aligned}$$

one readily arrives at a uniform order parameter, $\Delta_{\mathbf{k}}^{\alpha} = \Delta$, independent of the band index. A uniform order parameter across all bands has also been considered in Ref. [44].

In fact, in the weak coupling regime, only the gap near the Fermi level matters quantitatively. For the Lieb lattice, the Fermi level crosses only one of the three bands. In the opposite strong pairing regime, two-body physics becomes dominant so that the gap becomes quantitatively less important. This further justifies the adoption of a band-uniform pairing interaction, as a leading order approximation.

For the electron gas in a solid, there is *no natural way to create an on-site attractive interaction*, unlike the Coulomb repulsion in a repulsive Hubbard model. For the electron-phonon interaction, one may conceive that the attraction between neighboring sites is the strongest. This suggests that

one may use a short-range interaction as an approximation. While the optical lattice with cold atoms may see more flexibility, one eventually needs to find a way to simulate the real solid as well.

While one certainly can consider tunable inter- and intra-band interactions (possibly via tuning the inter-orbital and intra-orbital interaction), it is reasonable to consider a uniform interaction as a first step. Indeed, in other contexts, effects of tunable inter- and intra-band interactions have been studied for multiband systems in the literature [54–57]. It should be noted, however, that in a typical multiband superconductor, such as MgB_2 [58], iron pnictides and iron selenides [59], the multibands are often associated with multiple topologically disconnected Fermi surface sheets that are present simultaneously. This is very different from the Lieb lattice we consider. For these multi-Fermi surface cases, band selective pairing interactions, and hence band dependent pairing gaps, are more appropriate, as observed in ARPES measurements [59, 60].

Finally, we note that the ‘‘orbital’’ in the Lieb lattice refers to the sublattice sites, which is different from the electronic orbital states of the same atoms, such as the d_{xy} and d_{xz} orbitals of Fe in iron-based superconductors. Nevertheless, both types of ‘‘multi-orbitals’’ lead to multi-bands.

Appendix B: Derivation of the $\bar{\Delta}(\bar{g})$ relation for $n > 2$, expressed in terms of the Lambert W function

For $n > 2$, we substitute the (over) simplified model of $\bar{\rho}(\bar{\varepsilon})$ into the gap equation, and get

$$\begin{aligned} \frac{1}{|\bar{g}|} &= \int_0^1 d\bar{\varepsilon} \frac{\bar{\rho}(\bar{\varepsilon})}{2\sqrt{(\bar{\varepsilon} - \bar{\mu})^2 + \bar{\Delta}^2}} \\ &= 8 \int_{-\frac{1}{2}}^0 d\bar{\varepsilon} \frac{1}{2\sqrt{\bar{\varepsilon}^2 + \bar{\Delta}^2}} + (n-2) \frac{1}{2\bar{\Delta}} \\ &= 4 \sinh^{-1} \left(\frac{1}{2\bar{\Delta}} \right) + (n-2) \frac{1}{2\bar{\Delta}} \\ &\approx 4 \ln \left(\frac{1}{\bar{\Delta}} \right) + (n-2) \frac{1}{2\bar{\Delta}} \end{aligned} \quad (\text{B1})$$

Here $\bar{\mu} = 1/2$ and the second term on the right hand side comes from the fermion occupation in the flat band, given by $n - 2$. We have assumed a small $\bar{\Delta}$ in the weak coupling regime. Therefore,

$$\frac{n-2}{8} e^{1/4|\bar{g}|} = \frac{n-2}{8\bar{\Delta}} e^{\frac{n-2}{8\bar{\Delta}}}.$$

Using the definition of the Lambert function, $x = \mathcal{W}(x)e^{\mathcal{W}(x)}$, finally we obtain

$$\frac{n-2}{8\bar{\Delta}} = \mathcal{W} \left(\frac{n-2}{8} e^{1/4|\bar{g}|} \right),$$

namely,

$$\bar{\Delta} = \frac{(n-2)/8}{\mathcal{W}(\frac{n-2}{8} \exp(\frac{1}{4|\bar{g}|}))}.$$

For small $|x| \leq 1/e$, the principal branch can be Taylor expanded as [61]

$$\mathcal{W}(x) = \sum_{n=1}^{\infty} \frac{(-n)^{n-1}}{n!} x^n \approx x - x^2 + \frac{3}{2}x^3.$$

Relevant to our study is the large x limit, which corresponds to small $\bar{\Delta}$. In this case, $\mathcal{W}(x) \approx \ln(x) - \ln(\ln(x))$. Therefore, to leading order, we have $\bar{\Delta} \approx \frac{n-2}{2}|\bar{g}|$ for $n > 2$ in the weak

interaction regime.

Note that for $n < 2$, the 2nd term in Eq. (B1) is absent, and $\bar{\mu} = n/4$ based on the simplified model of $\bar{\rho}(\bar{\varepsilon})$. Then we obtain

$$\bar{\Delta} \approx \sqrt{n(1-n/4)} e^{-1/4|\bar{g}|},$$

which recovers the conventional exponential BCS behavior. At $n = 2$, it connects smoothly with the solution of Eq. (B1).

-
- [1] Q. J. Chen, J. Stajic, S. N. Tan, and K. Levin, BCS–BEC crossover: From high temperature superconductors to ultracold superfluids, *Phys. Rep.* **412**, 1 (2005).
- [2] I. Bloch, J. Dalibard, and W. Zwerger, Many-body physics with ultracold gases, *Rev. Mod. Phys.* **80**, 885 (2008).
- [3] W. Zwerger, ed., *The BCS-BEC Crossover and the Unitary Fermi Gas* (Springer Berlin Heidelberg, 2012).
- [4] R. A. Hart, P. M. Duarte, T.-L. Yang, X. Liu, T. Paiva, E. Khatami, R. T. Scalettar, N. Trivedi, D. A. Huse, and R. G. Hulet, Observation of antiferromagnetic correlations in the Hubbard model with ultracold atoms, *Nature* **519**, 211+ (2015).
- [5] I. Bloch, Quantum coherence and entanglement with ultracold atoms in optical lattices, *Nature* **453**, 1016 (2008).
- [6] B. DeMarco and D. S. Jin, Onset of Fermi degeneracy in a trapped atomic gas, *Science* **285**, 1703 (1999).
- [7] M. Bartenstein, A. Altmeyer, S. Riedl, S. Jochim, C. Chin, J. H. Denschlag, and R. Grimm, Crossover from a molecular Bose-Einstein condensate to a degenerate Fermi gas, *Phys. Rev. Lett.* **92**, 120401 (2004).
- [8] J. Kinast, A. Turlapov, J. E. Thomas, Q. J. Chen, J. Stajic, and K. Levin, Heat capacity of a strongly interacting Fermi gas, *Science* **307**, 1296 (2005).
- [9] M. Zwierlein, A. Schirotzek, C. Schunck, and W. Ketterle, Fermionic superfluidity with imbalanced spin populations, *Science* **311**, 492 (2006).
- [10] G. Partridge, W. Li, R. Kamar, Y. Liao, and R. Hulet, Pairing and phase separation in a polarized Fermi gas, *Science* **311**, 503 (2006).
- [11] D. Jaksch, C. Bruder, J. I. Cirac, C. W. Gardiner, and P. Zoller, Cold bosonic atoms in optical lattices, *Phys. Rev. Lett.* **81**, 3108 (1998).
- [12] C. Chin, R. Grimm, P. Julienne, and E. Tiesinga, Feshbach resonances in ultracold gases, *Rev. Mod. Phys.* **82**, 1225 (2010).
- [13] T. Timusk and B. Statt, The pseudogap in high-temperature superconductors: an experimental survey, *Rep. Prog. Phys.* **62**, 61 (1999).
- [14] Q. J. Chen, I. Kosztin, B. Jankó, and K. Levin, Pairing fluctuation theory of superconducting properties in underdoped to overdoped cuprates, *Phys. Rev. Lett.* **81**, 4708 (1998).
- [15] Y. Cao, V. Fatemi, S. Fang, K. Watanabe, T. Taniguchi, E. Kaxiras, and P. Jarillo-Herrero, Unconventional superconductivity in magic-angle graphene superlattices, *Nature* **556**, 43 (2018).
- [16] N. B. Kopnin, T. T. Heikkilä, and G. E. Volovik, High-temperature surface superconductivity in topological flat-band systems, *Phys. Rev. B* **83**, 220503(R) (2011).
- [17] V. J. Kauppila, F. Aikebaier, and T. T. Heikkilä, Flat-band superconductivity in strained Dirac materials, *Phys. Rev. B* **93**, 214505 (2016).
- [18] Y.-F. Wang, Z.-C. Gu, C.-D. Gong, and D. N. Sheng, Fractional quantum Hall effect of hard-core bosons in topological flat bands, *Phys. Rev. Lett.* **107**, 146803 (2011).
- [19] W. Beugeling, J. C. Everts, and C. Morais Smith, Topological phase transitions driven by next-nearest-neighbor hopping in two-dimensional lattices, *Phys. Rev. B* **86**, 195129 (2012).
- [20] Z. Q. Wang, G. Chaudhary, Q. J. Chen, and K. Levin, Quantum geometric contributions to the bkt transition: Beyond mean field theory, *Phys. Rev. B* **102**, 184504 (2020).
- [21] E. H. Lieb, Two theorems on the Hubbard model, *Phys. Rev. Lett.* **62**, 1201 (1989).
- [22] K. Sun, Z. Gu, H. Katsura, and S. Das Sarma, Nearly flatbands with nontrivial topology, *Phys. Rev. Lett.* **106**, 236803 (2011).
- [23] E. Tang, J.-W. Mei, and X.-G. Wen, High-temperature fractional quantum Hall states, *Phys. Rev. Lett.* **106**, 236802 (2011).
- [24] T. Neupert, L. Santos, C. Chamon, and C. Mudry, Fractional quantum Hall states at zero magnetic field, *Phys. Rev. Lett.* **106**, 236804 (2011).
- [25] S. Taie, H. Ozawa, T. Ichinose, T. Nishio, S. Nakajima, and Y. Takahashi, Coherent driving and freezing of bosonic matter wave in an optical Lieb lattice, *Sci. Adv.* **1**, 10.1126/sciadv.1500854 (2015).
- [26] F. Schafer, T. Fukuhara, S. Sugawa, Y. Takasu, and Y. Takahashi, Tools for quantum simulation with ultracold atoms in optical lattices, *Nat. Rev. Phys.* **2**, 411 (2020).
- [27] K.-E. Huhtinen, M. Tylutki, P. Kumar, T. I. Vanhala, S. Peotta, and P. Törmä, Spin-imbalanced pairing and Fermi surface deformation in flat bands, *Phys. Rev. B* **97**, 214503 (2018).
- [28] B. Cui, X. Zheng, J. Wang, D. Liu, S. Xie, and B. Huang, Realization of Lieb lattice in covalent-organic frameworks with tunable topology and magnetism, *Nat. Commun.* **11**, 66 (2020).
- [29] G. Palumbo and K. Meichanetzidis, Two-dimensional Chern semimetals on the Lieb lattice, *Phys. Rev. B* **92**, 235106 (2015).
- [30] K. Noda, A. Koga, N. Kawakami, and T. Pruschke, Ferromagnetism of cold fermions loaded into a decorated square lattice, *Phys. Rev. A* **80**, 063622 (2009).
- [31] K. Noda, K. Inaba, and M. Yamashita, Magnetism in the three-dimensional layered Lieb lattice: Enhanced transition temperature via flat-band and van Hove singularities, *Phys. Rev. A* **91**, 063610 (2015).
- [32] W. Nie, D. Zhang, and W. Zhang, Ferromagnetic ground state of the SU(3) Hubbard model on the Lieb lattice, *Phys. Rev. A* **96**, 053616 (2017).
- [33] N. Swain and M. Karmakar, Strain-induced superconductor-insulator transition on a Lieb lattice, *Phys. Rev. Res.* **2**, 023136 (2020).
- [34] V. I. Iglovikov, F. Hébert, B. Grémaud, G. G. Batrouni, and R. T. Scalettar, Superconducting transitions in flat-band systems, *Phys. Rev. B* **90**, 094506 (2014).

- [35] W. Zhu, S. Hou, Y. Long, H. Chen, and J. Ren, Simulating quantum spin Hall effect in the topological Lieb lattice of a linear circuit network, *Phys. Rev. B* **97**, 075310 (2018).
- [36] E. Sadeghi and H. Rezania, Spin-orbit coupling effects on transport properties of electronic Lieb lattice in the presence of magnetic field, *Sci. Rep.* **12**, 8523 (2022).
- [37] A. Pires, Transport on the ferromagnetic Lieb lattice, *J. Magn. Mater.* **547**, 168941 (2022).
- [38] L. Chen, T. Mazaheri, A. Seidel, and X. Tang, The impossibility of exactly flat non-trivial Chern bands in strictly local periodic tight binding models, *J. Phys. A: Math. Theor.* **47**, 152001 (2014).
- [39] C.-C. Chien, Q. J. Chen, and K. Levin, Fermions with attractive interactions on optical lattices and implications for correlated systems, *Phys. Rev. A* **78**, 043612 (2008).
- [40] Y. M. Che, J. B. Wang, and Q. J. Chen, Reentrant superfluidity and pair density wave in single-component dipolar Fermi gases, *Phys. Rev. A* **93**, 063611 (2016).
- [41] L. Sun, J. B. Wang, X. Chu, and Q. J. Chen, Pairing phenomena and superfluidity of atomic Fermi gases in a two-dimensional optical lattice: Unusual effects of lattice-continuum mixing, *Annalen der Physik* **534**, 2100511 (2022).
- [42] L. Sun and Q. J. Chen, Ground states of atomic Fermi gases in a two-dimensional optical lattice with and without population imbalance, *Phys. Rev. A* **106**, 013317 (2022).
- [43] A. Julku, S. Peotta, T. I. Vanhala, D.-H. Kim, and P. Törmä, Geometric origin of superfluidity in the Lieb-lattice flat band, *Phys. Rev. Lett.* **117**, 045303 (2016).
- [44] N. Chamel, S. Goriely, J. M. Pearson, and M. Onsi, Unified description of neutron superfluidity in the neutron-star crust with analogy to anisotropic multiband BCS superconductors, *Phys. Rev. C* **81**, 045804 (2010).
- [45] Q. J. Chen, Z. Q. Wang, R. Boyack, S. L. Yang, and K. Levin, When superconductivity crosses over: From BCS to BEC (2022), arXiv:2208.01774 [cond-mat.supr-con].
- [46] D. J. Scalapino, S. R. White, and S. C. Zhang, Superfluid density and the drude weight of the Hubbard model, *Phys. Rev. Lett.* **68**, 2830 (1992).
- [47] I. Kosztin, Q. J. Chen, B. Jankó, and K. Levin, Relationship between the pseudo- and superconducting gaps: Effects of residual pairing correlations below T_c , *Phys. Rev. B* **58**, R5936 (1998).
- [48] L. Liang, T. I. Vanhala, S. Peotta, T. Siro, A. Harju, and P. Törmä, Band geometry, Berry curvature, and superfluid weight, *Phys. Rev. B* **95**, 024515 (2017).
- [49] Note that the (n_s/m) tensor has to be calculated as a whole, not n_s and m separately.
- [50] K.-E. Huhtinen, J. Herzog-Arbeitman, A. Chew, B. A. Bernevig, and P. Törmä, Revisiting flat band superconductivity: Dependence on minimal quantum metric and band touchings, *Phys. Rev. B* **106**, 014518 (2022).
- [51] H. Guo, Y. He, C.-C. Chien, and K. Levin, Compressibility in strongly correlated superconductors and superfluids: From the BCS regime to Bose-Einstein condensates, *Phys. Rev. A* **88**, 043644 (2013).
- [52] X. Liu, Y. X. Chong, R. Sharma, and J. C. S. Davis, Discovery of a Cooper-pair density wave state in a transition-metal dichalcogenide, *Science* **372**, 1447 (2021).
- [53] L. F. Zhang, Y. M. Che, J. B. Wang, and Q. J. Chen, Exotic superfluidity and pairing phenomena in atomic Fermi gases in mixed dimensions, *Sci. Rep.* **7**, 12948 (2017).
- [54] M. Takahashi, T. Mizushima, and K. Machida, Multiband effects on Fulde-Ferrell-Larkin-Ovchinnikov states of Pauli-limited superconductors, *Phys. Rev. B* **89**, 064505 (2014).
- [55] G. Litak, T. Örd, K. Rágo, and A. Vargunin, Band filling effects on coherence lengths and penetration depth in the two-orbital negative- u hubbard model of superconductivity, *Physica C: Superconductivity* **483**, 30 (2012).
- [56] E. M. Nica, R. Yu, and Q. Si, Orbital-selective pairing and superconductivity in iron selenides, *npj Quant. Mater.* **2**, 24 (2017).
- [57] W.-M. Huang and H.-H. Lin, Pairing mechanism in multiband superconductors, *Sci. Rep.* **10**, 7439 (2020).
- [58] S. Tsuda, T. Yokoya, and S. Shin, Recent photoemission studies on MgB_2 and related materials, *Physica C* **456**, 126 (2007).
- [59] R. M. Fernandes, A. I. Coldea, H. Ding, I. R. Fisher, P. J. Hirschfeld, and G. Kotliar, Iron pnictides and chalcogenides: a new paradigm for superconductivity, *Nature* **601**, 35 (2022).
- [60] H. Ding, P. Richard, K. Nakayama, K. Sugawara, T. Arakane, Y. Sekiba, A. Takayama, S. Souma, T. Sato, T. Takahashi, Z. Wang, X. Dai, Z. Fang, G. F. Chen, J. L. Luo, and N. L. Wang, Observation of Fermi-surface-dependent nodeless superconducting gaps in $\text{Ba}_{0.6}\text{K}_{0.4}\text{Fe}_2\text{As}_2$, *Europhys. Lett.* **83**, 47001 (2008).
- [61] T. P. Dence, A brief look into the Lambert W function, *Appl. Math.* **4**, 887 (2013).